



HAL
open science

Thermomechanical performance of blended metakaolin-GGBS alkali-activated foam concrete

Gabriel Samson, Martin Cyr, Xiao Xiao Gao

► **To cite this version:**

Gabriel Samson, Martin Cyr, Xiao Xiao Gao. Thermomechanical performance of blended metakaolin-GGBS alkali-activated foam concrete. *Construction and Building Materials*, 2017, 157, pp.982-993. 10.1016/j.conbuildmat.2017.09.146 . hal-01756696

HAL Id: hal-01756696

<https://hal.science/hal-01756696>

Submitted on 2 Apr 2018

HAL is a multi-disciplinary open access archive for the deposit and dissemination of scientific research documents, whether they are published or not. The documents may come from teaching and research institutions in France or abroad, or from public or private research centers.

L'archive ouverte pluridisciplinaire **HAL**, est destinée au dépôt et à la diffusion de documents scientifiques de niveau recherche, publiés ou non, émanant des établissements d'enseignement et de recherche français ou étrangers, des laboratoires publics ou privés.

Thermomechanical performance of blended metakaolin-GGBS alkali-activated foam concrete

Gabriel Samson¹, Martin Cyr¹, Xiao Xiao Gao²

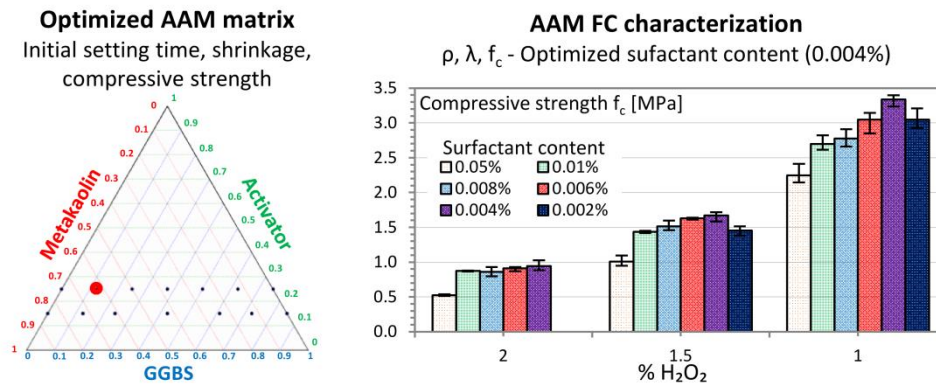
¹ *LMDC, INSAT/UPS Génie Civil, 135 Avenue de Rangueil, 31077 Toulouse cedex 04 France.*

² *ECOCEM, 3rd Floor Port view House, Grand Canal Docks, Dublin 4, Ireland*

Abstract

This study aims to synthesize, at ambient temperature, blended metakaolin-ground granulated blast furnace slag (MK-GGBS) foam concrete (FC) presenting good thermomechanical performance for use as self-bearing insulation material. First, a binder composition that could be used for MK-GGBS FC production was identified. Fourteen paste formulations were produced and analysed to determine the best proportions of MK, GGBS and activator to be used in an alkali-activated material (AAM) FC matrix. Certain requirements were specified for the fresh paste (initial setting time > 180 minutes) and solid materials (high compressive strength and moderate shrinkage) to be used for FC production. The optimized mix was then employed for AAM FC production by using an H₂O₂ blowing agent (gas-foaming method). The influence of two main parameters (H₂O₂ and surfactant contents) on AAM FC properties (density, porous structure, thermal conductivity and compressive strength) were investigated. The thermomechanical performances of the AAM FCs produced were good compared to FC performances found in the literature. FC density mostly depends on H₂O₂ content. The FC porous structure depends strongly on both H₂O₂ and surfactant contents. High surfactant content FCs have a thin homogenous porous structure. At constant density, FC compressive strength depends on the surfactant content. An optimized surfactant content maximizing FC compressive strength at constant density was identified.

Graphical abstract



Highlights

- Optimized proportions between metakaolin, GGBS and activator were identified.
- H_2O_2 gas-off lasts 180 minutes. AAMs paste initial setting time must start after.
- Lightweight AAMs were obtained with density from 264 to 480 kg/m^3 .
- The foam concrete porous structure depends on both H_2O_2 and surfactant contents.
- An optimized surfactant content (0.004%) maximized FC compressive strength.

Keywords

Alkali-activated material (AAM), metakaolin (MK), GGBS, compressive strength, thermal conductivity, optimized surfactant content

Corresponding author

Martin Cyr, cyr@insa-toulouse.fr

Funding

This research did not receive any specific grant from funding agencies in the public, commercial, or not-for-profit sectors.

1 Introduction

During the last decades, there was a massive growing interest on research on alkali-activated materials (AAMs). These researches prove that these materials can be successfully used to produce load-bearing materials with good properties [1,2]. AAMs are produced by mixing aluminosilicate precursors (e.g. metakaolin (MK) or fly ash (FA)) or calcium aluminosilicate precursors (e.g. ground granulated blast furnace slag (GGBS)) rich in SiO_2 , Al_2O_3 (and CaO) activated by a highly alkaline solution (usually NaOH , KOH or sodium silicate solution). Most of AAMs are based on aluminosilicate precursors that are industrial by-products. Using these precursors can reduce the embodied CO_2 if mix design and raw materials selection are carried out with a view towards optimisation of environmental performance [3]. Moreover using these precursors increase the use of waste materials, thus avoiding their storage in a landfill and the resulting pollution problems. AAMs present good mechanical properties and fire resistance [4]. A few studies showed that mixing GGBS and MK present some advantages. These studies were performed on MK-GGBS paste [5–9] and mortar [10]. Adding GGBS to MK-based geopolymers provides an improvement in mechanical properties [5,9] and reduces shrinkage [9]. Samson et al. [9] produced and characterized blended AAMs based on flash-calcined MK and GGBS. The influence of compositions (MK, GGBS and activator contents) on initial setting time, shrinkage, mass loss and compressive strength were investigated.

The relatively new development of AAMs (compared to OPC) explains why only a few studies have been conducted on AAM FCs. Most FCs are made with Ordinary Portland cement (OPC) alone or with additions [11–13]. The main information on AAM FCs available in the literature is summarized in Table 1 (aluminosilicate precursors, alkaline activation, production method, surfactant, blowing agent, density, compressive strength and thermal conductivity). Most of the AAM FCs reported in the literature were produced with fly ash (FA) [14–21] and needed to be thermally cured. AAM FCs were also successfully prepared with a mix of FA and GGBS [22,23] and some were made with MK [24,25] or GGBS [26,27] but none have been made with blended MK-GGBS binder. The vast majority of AAM FCs are produced with the gas-foaming method [15–19,21,24,25,27–29].

This study aimed to synthesize and to characterize blended MK-GGBS FC presenting good thermomechanical performance for use as self-bearing insulation material. The fact that some AAM FCs needs to be thermally treated to achieve reasonable properties is a major problem for industrial applications. Alternative binders proposed by researchers have to be produced under ambient conditions

if they are to be economically and environmentally competitive. This explains why the AAM FCs presented in this study were produced at ambient temperature. The first step of this study was to identify a binder composition that could be used for MK-GGBS FC production. As far as we know, no blended MK-GGBS FC studies have been reported in the literature. This paste had to have controlled initial setting time, reasonable shrinkage and good mechanical properties. The results obtained by Samson et al. [9] are summarized and used to identify the optimized binder for AAM FCs production. Once identified, this optimal binder composition was then employed to produce FC with controlled density and porous structure. The influence of two main composition parameters (H_2O_2 and surfactant contents) on AAM FC density, porous structure, compressive strength and thermal conductivity were investigated. The thermomechanical performances of the AAM FCs produced were then compared to the performances of FCs found in the literature.

Table 1. Review of FC composition, fresh paste density and thermomechanical properties.

| Ref. number | Main author | Composition | Alkaline activator | Production process | Surfactant | Blowing agent | Curing | Apparent density [kg/m ³] | Compressive strength [MPa] | Compressive strength test Dimensions + age | Thermal conductivity [W/(m.K)] |
|-------------|-------------|--------------------------------------|--|-----------------------------|--|------------------------------------|-------------------------------|---------------------------------------|----------------------------|---|--------------------------------|
| [15] | Sanjayan | FA | NaOH solution + sodium silicate | Gas-foaming | no | Al | 24h at 60°C after unmoulding | 403 - 1309 | 0.9 - 4.35 | Cubic 50 mm | no |
| [16] | Kamseu | Rice husk (R) and volcanic (P) ashes | NaOH solution | Gas-foaming | no | Al | no | no | no | no | 0.15 - 0.4 |
| [17] | Hlaváček | FA | NaOH + sodium metasilicate solution | Gas-foaming | no | Al | 2h at 22°C + 12h at 80°C | 400 - 800 | 4.5 - 6 | Cubic 30 mm | 0.145 - 0.18 |
| [18] | Ducman | FA | Sodium silicate solution + NaOH solution | Gas-foaming | no | Al - H ₂ O ₂ | 24h at 70°C | 610 - 1000 | 2.9 - 9.3 | Cubic 20 mm - 4 days | no |
| [19] | Masi | FA | Sodium aluminate | Gas-foaming and mix-foaming | Sika lightcrete 02 (40% of fatty acid, amide and sodium salt of C ₁₄ -C ₁₆ sulphonic acid) | Al - H ₂ O ₂ | 24h at 70°C | 720 - 1320 | 1.6 - 7.2 | Cylinder 50 mm height - 20 mm diameter - 7 days | no |
| [21] | Korat | FA | Sodium silicate | Gas-foaming | SDS | H ₂ O ₂ | 24h at 70°C | 580 - 1340 | 2.6 - 12.2 | Cubic 20 mm | no |
| [22] | Zhang | 70% FA - 30% GGBS | NaOH solution and a sodium silicate solution | Pre-foaming | Probably...no details | no | 24h at 40°C - 27 days ambient | ≈ 350 - 650 | 4 - 50 | Cylinder 53 × 105 mm | no |

| | | | | | | | | | | | |
|------|-----------------------|--------------------------------------|--|-------------|--|-------------------------------|---|------------|----------------------------------|--|---|
| | | | | | | | temperature in moulds | | | | |
| [23] | Zhang | FA - GGBS | NaOH + sodium silicate solution | Pre-foaming | No details | no | 24h at 40°C - 27 days at ambient conditions in moulds | 580 - 1630 | 3.3 - 49.0 For p [720 - 1630] | Cylinder 100 mm diameter – 200 mm height - 28 days | After 6h of drying at 80°C 0.14 - 0.47 |
| [24] | Palmero | MK | NaOH, KOH sodium silicate solution and SiO ₂ nanopowder | Gas-foaming | | H ₂ O ₂ | Room temperature or 65°C for 24 h until testing | 330 - 690 | 2 - 5.2 | 14 days | 0.13 - 0.17 |
| [25] | Lassinantti Gualtieri | MK | Phosphoric acid | Gas-foaming | Marlipal = non ionic surfactant | Natural limestone | 24h at 60°C | 580 - 730 | no | no | 0.07 - 0.091 |
| [26] | Yang | GGBS | three types of alkali activators: 10% Ca(OH) ₂ and 4% Mg(NO ₃) ₂ , 5% Ca(OH) ₂ and 6.5% Na ₂ SiO ₃ , and 2.5% Ca(OH) ₂ and 6.5% Na ₂ SiO ₃ | Pre-foaming | protein with enzymatic active components | no | Room temperature | 325 - 492 | 0.5 - 1.97 | Cylinder 100 mm diameter - 200 mm height - 7 and 28 days | 0.088 - 0.129 |
| [27] | Esmaily | GGBS | Sodium silicate | Gas-foaming | Microair + fat acid + SLS | Al | 87°C | 700 - 1160 | 0.9 - 15.3 | Cubic 50 mm | no |
| [28] | Novais | MK - FA | hydrated sodium silicate and NaOH | Gas-foaming | no | H ₂ O ₂ | 24h at 60°C - 65% RH | 440 - 1170 | 0.14 - 20.67 | Cylinder 220 480mm | 0.082 - 0.227 |
| [29] | Dembovska | MK - Glass waste – stell-plant waste | Sodium silicate | Gas-foaming | no | aluminium nitride | 24h at 80°C | 380 - 470 | 1.1- 2.0 | Cubic 40 mm | 0.14 - 0.15 |

2 Materials

2.1 Binders

The MK used in this study was produced in the south of France (Argéco Développement®). One of the main drawbacks of the MK AAMs is a tendency towards drying shrinkage and cracking [5,30]. MK density and specific surface are 2500 kg/m³ and 14000 m²/kg (BET analysis) respectively. XRD, ICP and Rietveld analysis performed by Pouhet [30] show that this MK has a high impurity content (quartz, anatase, mullite, kaolinite). The different oxide contents were obtained by ICP analysis and are presented in Table 2. The analyses reveal that the amorphous proportions of SiO₂ and Al₂O₃ were respectively 29 and 24% (Table 2).

The GGBS used in this study was produced in France at Fos sur Mer (Ecocem®) and complied with EN 151-67-1. GGBS density and Blaine surface are 2900 kg/m³ and 4450 m²/kg respectively. The activity index at 28 days was 98% (EN 196-1). A diffusion hump seen on the XRD diagram confirmed that the GGBS was almost totally amorphous. Detailed physical properties as well as particle size distributions of MK and GGBS are given in [9].

Table 2. Raw material chemical composition.

| | | SiO ₂ | Al ₂ O ₃ | CaO | MgO | Fe ₂ O ₃ | K ₂ O | Na ₂ O | TiO ₂ | SO ₃ | H ₂ O | LOI | Amorphous phase | |
|-------------------|---|------------------|--------------------------------|------|------|--------------------------------|------------------|-------------------|------------------|-----------------|------------------|------|------------------|--------------------------------|
| | | | | | | | | | | | | | SiO ₂ | Al ₂ O ₃ |
| Metakaolin | % | 68.1 | 24.1 | 0.20 | 0.22 | 3.73 | 0.35 | 0.08 | 1.14 | 0.03 | - | 1.83 | 29 | 24 |
| GGBS | % | 37.2 | 11.3 | 43.4 | 6.6 | 0.7 | 0.3 | 0.2 | 0.6 | 0.03 | - | - | 37.2 | 11.3 |
| Alkaline solution | % | 27.5 | - | - | - | - | - | 16.9 | - | - | 55.6 | - | - | - |

2.2 Activator, blowing agent and surfactant

The alkali activation was performed with a commercial sodium silicate solution (Betol 47T - Woellner®) which composition is detailed in Table 2. The SiO₂/Na₂O molar ratio was 1.68. The dry extract (44.4%) corresponded to the material of the alkaline solution (commercial solution) that remained if all the water was evaporated (55.6%). A small amount of soda NaOH (3.2% of the mass of the alkaline solution) was added to improve the activation. The dry extract of the alkaline solution plus NaOH is referred to as the activator. The AAM FC porosity was created with hydrogen peroxide H₂O₂ (purity 50% - Solvay®) as blowing agent. A commercial surfactant was employed to stabilize the AAM FC porous structure before MK-GGBS matrix setting.

3 Methods

3.1 Mix design

Fourteen paste formulations were produced and analysed to determine the best proportions of MK, GGBS and activator to be used as the matrix for the AAM FC. The details of this mix-design was presented on [9] for three types of blended AAMs (26 compositions). MK was mixed with GGBS because pure GGBS AAMs are subject to high shrinkage [31]. These mixes are presented in a ternary diagram (Figure 1) and in Table 4. It was built by changing the proportions of the three raw materials: MK, GGBS and activator (dry extract of alkaline solution + NaOH). Hereafter, the samples will be designated as: $A_iMK_jGGBS_k$ where A is the activator and i the associated percentage, j is the MK percentage, k is the GGBS percentage. Each sample verified $i + j + k = 100$. All the samples had the same water to binder mass ratio, $W/B = 0.36$. This minimum W/B ratio was evaluated with preliminary tests on the two samples that only contain MK ($A_{25}MK_{75}$ and $A_{15}MK_{85}$ - Table 3). MK particles led to higher water demand than GGBS or FA [35] because of the plate-like morphology of the MK particles. The minimum W/B ($W/B = 0.36$) corresponded to the minimum fluidity required to fill all the moulds without vibration.

The binder comprised the dry powders (MK and GGBS) and the activator (dry extract of the alkaline activator solution + NaOH). The water came from the alkaline solution and a suitable amount of water was added to satisfy the constant W/B ratio for each mix (Table 3). When the activator percentage was 15%, the percentage of water coming from the alkaline solution was 49.5% (50.5% from water addition). With 25% of activator, 84.2% of the water came from the alkaline solution.

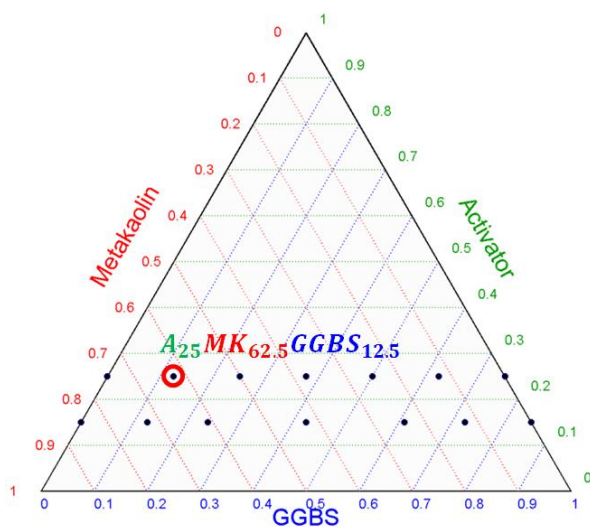


Figure 1. Mix-design: Ternary systems containing MK, GGBS and activator.

Table 3. AAM compositions and test results.

| Unit | Ternary composition | | | Water | | Molar ratio | | | | Setting | Shrinkage | | | | | Compressive strength | | |
|---|---------------------|------|------|---------------------|---------------------------|--|-------------------------------------|--|------------------------------------|---------|---------------------|-----|-----|-----|-----|----------------------|------|-------|
| | Activator* | MK | GGBS | Alkaline solution** | Added *** (pure water) | SiO ₂ /Al ₂ O ₃ | SiO ₂ /Na ₂ O | Na ₂ O/Al ₂ O ₃ | H ₂ O/Na ₂ O | Ts | Δl / l ₀ | | | | | f _c | | |
| | % | % | % | % | % | | | | | min | % | | | | | MPa | | |
| Time [days] | - | - | - | - | - | | | | | | 2 | 7 | 14 | 21 | 28 | 1 | 7 | 28 |
| A ₂₅ MK ₇₅ | 25.0 | 75.0 | 0.0 | 84.2 | 15.8 | 3.46 | 3.83 | 0.90 | 12.52 | 360 | 2.2 | 2.3 | 2.3 | 2.4 | 2.4 | 21.4 | 50.5 | 53.2 |
| A ₁₅ MK ₈₅ | 15.0 | 85.0 | 0.0 | 49.5 | 50.5 | 2.80 | 5.81 | 0.48 | 20.75 | 265 | 1.2 | 1.2 | 1.2 | 1.3 | 1.3 | 2.5 | 7.7 | 10.4 |
| A ₂₅ MK _{62.5} GGBS _{12.5} | 25.0 | 62.5 | 12.5 | 84.2 | 15.8 | 3.90 | 4.04 | 0.99 | 12.53 | 300 | 0.8 | 0.8 | 0.9 | 0.8 | 0.9 | 31.6 | 66.5 | 69.8 |
| A ₂₅ MK ₅₀ GGBS ₂₅ | 25.0 | 50.0 | 25.0 | 84.2 | 15.8 | 4.44 | 4.05 | 1.10 | 12.54 | 160 | 1.0 | 1.2 | 1.3 | 1.3 | 1.3 | 45.5 | 58.6 | 62.7 |
| A ₂₅ MK _{37.5} GGBS _{37.5} | 25.0 | 37.5 | 37.5 | 84.2 | 15.8 | 5.11 | 4.16 | 1.23 | 12.55 | 115 | 1.0 | 1.7 | 1.7 | 1.9 | 1.9 | 41.0 | 55.3 | 65.3 |
| A ₂₅ MK ₂₅ GGBS ₅₀ | 25.0 | 25.0 | 50.0 | 84.2 | 15.8 | 5.95 | 4.28 | 1.39 | 12.57 | 90 | 1.1 | 2.5 | 2.9 | 3.0 | 3.1 | 31.6 | 57.6 | 79.3 |
| A ₂₅ MK _{12.5} GGBS _{62.5} | 25.0 | 12.5 | 62.5 | 84.2 | 15.8 | 7.07 | 4.39 | 1.61 | 12.58 | 105 | 1.3 | 3.3 | 3.7 | 3.8 | 3.8 | 15.5 | 47.6 | 82.3 |
| A ₁₅ MK _{72.5} GGBS _{12.5} | 15.0 | 72.5 | 12.5 | 49.5 | 50.5 | 3.13 | 6.00 | 0.52 | 20.78 | 115 | 0.3 | 0.4 | 0.4 | 0.5 | 0.5 | 16.4 | 36.9 | 47.1 |
| A ₁₅ MK ₆₁ GGBS ₂₄ | 15.0 | 61.0 | 24.0 | 49.5 | 50.5 | 3.48 | 6.17 | 0.56 | 20.81 | 65 | 0.3 | 0.4 | 0.4 | 0.5 | 0.5 | 26.8 | 38.2 | 50.8 |
| A ₁₅ MK _{42.5} GGBS _{42.5} | 15.0 | 42.5 | 42.5 | 49.5 | 50.5 | 4.20 | 6.45 | 0.65 | 20.87 | 50 | 0.9 | 1.0 | 1.1 | 1.1 | 1.1 | 21.7 | 34.0 | 46.3 |
| A ₁₅ MK ₂₄ GGBS ₆₁ | 15.0 | 24.0 | 61.0 | 49.5 | 50.5 | 5.19 | 6.74 | 0.77 | 20.92 | 40 | 2.0 | 2.3 | 2.4 | 2.4 | 2.5 | 16.0 | 31.5 | 92.8 |
| A ₁₅ MK _{12.5} GGBS _{72.5} | 15.0 | 12.5 | 72.5 | 49.5 | 50.5 | 6.91 | 6.91 | 0.87 | 20.95 | 40 | 3.1 | 3.9 | 4.1 | 4.2 | 4.2 | 17.9 | 66.5 | 98.6 |
| A ₂₅ GGBS ₇₅ | 25.0 | 0.0 | 75.0 | 84.2 | 15.8 | 8.60 | 4.50 | 1.91 | 12.59 | 70 | 1.1 | 2.8 | 3.4 | 3.6 | 3.8 | 44.5 | 67.3 | 83.7 |
| A ₁₅ GGBS ₈₅ | 15.0 | 0.0 | 85.0 | 49.5 | 50.5 | 7.19 | 7.10 | 1.01 | 20.99 | 45 | 2.4 | 3.9 | 4.1 | 4.2 | 4.3 | 32.2 | 80.4 | 110.5 |

* dry extract of the alkaline solution + NaOH ** water from the alkaline solution ***Added water is used to satisfy constant W/B = 0.36 for each sample

3.2 AAM production

The production of the blended AAMs started with dry mixing of the MK and GGBS. Soda was diluted in the additional water and this solution was mixed with the alkaline solution. The resulting liquid was added to the powder (at the initial time, $t = 0$) and the liquid and powder were mixed together for 1 minute at low speed then 2 minutes at high speed using an ordinary mixer (Automix 65 - Controls®). The paste was then cast in the different moulds (Table 4). To prevent water transfer, the moulds were covered with plastic sheets. They were placed in a room at 20°C for 24h before unmoulding. The moulds used for AAM production and the AAM characterization schedule are presented in Table 4.

Table 4. AAM characterization.

| Test | Quantity measured | Moulds | Time [days] |
|----------------------|-------------------|--|---------------------|
| Initial setting time | mins | Truncated moulds - height 40 mm - diameter 80 mm | 0 |
| Compressive strength | MPa | Cubic (8 replicates) - height 20 mm | 1, 7, 28 |
| Shrinkage | % | Prismatic (3 replicates) - 20 x 20 x 160 mm | 1, 2, 7, 14, 21, 28 |
| Mass loss | % | | |

3.3 AAM characterization

The paste was characterized in the fresh state using an automatic Vicat device (Vicatrionic®) according to standard ASTM C191 - 01 [33]. The Vicat initial setting time was calculated as the time elapsed between the initial contact ($t = 0$) of dry powder and alkaline solution and the time when the penetration was 25 mm. Cubic and prismatic samples were unmoulded after 24 h. Cubic samples were stored in plastic bags to limit water loss. Prismatic samples were stored at 20°C and 50% RH without any protection. These unrestrained shrinkage conditions were quite severe for early age (24 h) samples. The shrinkage tests were performed by adapting the ASTM C 596 - 01 standard [34]. Prismatic samples (3 per composition) were weighed and measured at 1, 2, 7, 14, 21 and 28 days. The shrinkage was calculated as $(l-l_0)/l_0$ where l was the size of the samples and l_0 was the initial sample size after unmoulding. The mass loss was calculated as $(m-m_0)/m_0$ where m was the weight of the samples and m_0 was the initial sample weight after unmoulding. Compressive strength was measured after 1, 7 and 28 days on cubic samples. Eight samples were tested at each term (100 kN IGM® press, loading speed 0.5 kN/s) to have a good representative average of the compressive strength.

3.4 AAM FC production

Once the optimized mix was found, it was used to produce AAM FCs. MK, GGBS and the surfactant were dry mixed. The alkaline solution (commercial solution and added soda, as presented above) was added, followed by the same mixing process as for the paste. Immediately after paste production, the blowing agent H_2O_2 was added into the mineral suspension and additional mixing (30s at slow speed and 30s at high speed) was carried out to obtain a homogeneous paste. A semi-rigid plastic sheet was placed to cover the inner part of the cylindrical moulds used for FC production ($\phi = 118$ mm) so as to facilitate unmoulding. Preliminary tests were performed with aluminium powder but the off-gassing was too fast. The dioxygen was slowly released in the paste, making the FC volume increase over around 180 minutes. The moulds were then covered with plastic film to prevent water loss and placed in a room at $20^\circ C$ for a week. The influence of two main parameters: the H_2O_2 and surfactant contents, on AAM FC properties (density, porous structure, compressive strength and thermal conductivity) were investigated. The FC produced are referred to as HP_mS_n where HP means hydrogen peroxide (H_2O_2) and m is its percentage. S refers to surfactant and n its dosage. The different FC compositions and thermomechanical results are presented in Table 5. For each composition (H_2O_2 and surfactant contents) three FCs were produced. The different compositions are also presented in Table 5.

3.5 AAM FC characterization

The AAM FC specimens were unmoulded after 7 days. The FC specimens were around 200 mm high. The central part was sawed to obtain samples 118 mm high and 118 mm in diameter. The dimensions and weight of each sample were measured to obtain the unmoulded density ρ_{um} . Samples were then put in an oven at $40^\circ C$ for a week to dry. This step was necessary so that the thermal conductivity could be measured under dry conditions. Samples were weighed every day to observe the mass loss stabilization. After 7 days, the weights of all the samples had stabilized (dry density ρ_{dry}). The thermal conductivities were measured using the hot wire method (Neotim®). Three measurements were made for each sample, meaning that, for each FC composition, the thermal conductivity value presented in Table 5 is the average of nine measurements. The compressive strength was then determined with an IGM® press (100 kN, loading speed 0.2 kN/s). For each measurement, the coefficient of variation, CV (standard deviation of measurements divided by their average value) is presented to check FC production repeatability (Table 5).

Table 5. Properties of AAM FCs (the associated coefficient of variation is indicated under each result).

| | | HP ₂ S ₀ 05 | HP ₂ S ₀ 01 | HP ₂ S _{0.0} 08 | HP ₂ S _{0.0} 06 | HP ₂ S _{0.0} 04 | HP ₂ S _{0.0} 02 | HP ₂ S _{0.0} 01 | HP _{1.5} S ₀ 05 | HP _{1.5} S ₀ 01 | HP _{1.5} S _{0.0} 08 | HP _{1.5} S _{0.0} 06 | HP _{1.5} S _{0.0} 04 | HP _{1.5} S _{0.0} 02 | HP _{1.5} S _{0.0} 01 | HP ₁ S ₀ 05 | HP ₁ S ₀ 01 | HP ₁ S _{0.0} 08 | HP ₁ S _{0.0} 06 | HP ₁ S _{0.0} 04 | HP ₁ S _{0.0} 02 | HP ₁ S _{0.0} 01 | HP ₀ S ₀ | |
|---------------------------------------|-------------------|--------------------------------------|--------------------------------------|--|--|--|--|--|--|--|--|--|--|--|--|--------------------------------------|--------------------------------------|--|--|--|--|--|-----------------------------------|---|
| H ₂ O ₂ content | % | 2 | 2 | 2 | 2 | 2 | 2 | 2 | 1.5 | 1.5 | 1.5 | 1.5 | 1.5 | 1.5 | 1.5 | 1 | 1 | 1 | 1 | 1 | 1 | 1 | 1 | 0 |
| Surfactant content | % | 0.05 | 0.01 | 0.008 | 0.006 | 0.004 | 0.002 | 0.001 | 0.05 | 0.01 | 0.008 | 0.006 | 0.004 | 0.002 | 0.001 | 0.05 | 0.01 | 0.008 | 0.006 | 0.004 | 0.002 | 0.001 | 0 | |
| Unmoulded density | kg/m ³ | 308 | 327 | 327 | 331 | 339 | - | - | 392 | 410 | 412 | 412 | 413 | 418 | - | 526 | 554 | 553 | 562 | 559 | 559 | - | 1949 | |
| CV | % | 1.6 | 0.2 | 0.5 | 0.5 | 1.1 | - | - | 1.4 | 1.9 | 0.4 | 1.1 | 0.8 | 1.7 | - | 3.0 | 0.8 | 2.9 | 1.4 | 0.5 | 1.9 | - | 1.8 | |
| Dry density | kg/m ³ | 264 | 280 | 280 | 283 | 291 | - | - | 336 | 352 | 354 | 353 | 354 | 358 | - | 451 | 473 | 472 | 480 | 477 | 478 | - | 1673 | |
| CV | % | 1.5 | 0.3 | 0.4 | 0.4 | 1.8 | - | - | 1.4 | 1.6 | 0.5 | 1.1 | 0.7 | 1.6 | - | 3.1 | 1.0 | 3.1 | 1.4 | 0.4 | 1.8 | - | 2.2 | |
| Mass loss | % | 14.5 | 14.5 | 14.5 | 14.5 | 14.3 | - | - | 14.2 | 14.3 | 14.0 | 14.3 | 14.3 | 14.4 | - | 14.3 | 14.5 | 14.6 | 14.5 | 14.6 | 14.4 | - | 14.4 | |
| Thermal conductivity λ | W/(m.K) | 0.084 | 0.090 | 0.091 | 0.092 | 0.098 | - | - | 0.099 | 0.106 | 0.108 | 0.108 | 0.109 | 0.113 | - | 0.122 | 0.128 | 0.129 | 0.131 | 0.133 | 0.139 | - | 1.12 | |
| CV | % | 1.2 | 2.3 | 2.2 | 0.6 | 2.6 | - | - | 2.6 | 0.9 | 1.1 | 1.4 | 2.3 | 3.7 | - | 0.5 | 2.3 | 2.2 | 1.6 | 0.9 | 1.1 | - | 0.9 | |
| Compressive strength | MPa | 0.53 | 0.87 | 0.86 | 0.91 | 0.94 | - | - | 1.01 | 1.43 | 1.51 | 1.63 | 1.67 | 1.45 | - | 2.24 | 2.70 | 2.78 | 3.05 | 3.34 | 3.05 | - | 69.9 | |
| CV | % | 2.5 | 0.8 | 7.9 | 3.8 | 7.7 | - | - | 7.7 | 1.1 | 4.7 | 0.9 | 4.6 | 4.7 | - | 6.5 | 4.2 | 4.5 | 5.5 | 2.6 | 4.8 | - | 14.3 | |

4 Results

4.1 Identification of the optimal AAM composition

Some preliminary tests were performed to determine the maximum acceptable initial setting time of the paste. This corresponds to the duration of the gas production in the AAM paste (conversion of H_2O_2 to O_2). If the paste starts to set before the end of the off-gassing, the FC produced will present very poor mechanical properties as the internal off-gassing would create damage in the porous structure of the FC. Ideally, the paste should set immediately after the off-gassing finishes. At that moment, the FC has reached its maximal and final height (elevation in the mould) and is stabilized by the surfactant, which prevents excessive coalescence of bubbles. The preliminary tests indicated that the oxygen release took around 180 minutes. The initial setting time results are presented in Figure 2 (a):

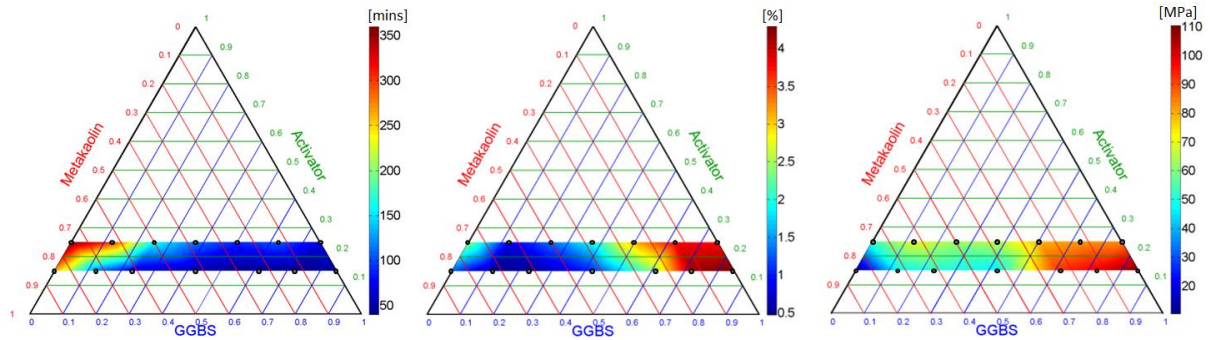


Figure 2. (a) Initial setting time, (b) 28 days shrinkage and (c) 28 days compressive strength of ternary systems containing MK, GGBS and activator.

Pure MK had the longest initial setting times (Figure 2 (a) - 360 and 265 minutes for $A_{25}GGBS_{75}$ and $A_{15}GGBS_{85}$, respectively). As observed by Gao et al. [35], for pure MK, the initial setting time was lower for smaller SiO_2/Al_2O_3 ratios. Adding GGBS significantly decreased the initial setting time. Pure GGBS AAMs presented very short initial setting times (Figure 2 (a) - 70 and 45 minutes for $A_{25}GGBS_{75}$ and $A_{15}GGBS_{85}$). Due to the high Ca content in GGBS, the reaction paths were very different from those obtained for MK or FA AAMs [36]. C-A-S-H gel was rapidly created, explaining the low initial setting time observed. The initial setting time had to be higher than 180 minutes, and only three mixes fulfilled this requirement ($A_{25}GGBS_{75}$, $A_{15}GGBS_{85}$ and $A_{25}MK_{62.5}GGBS_{12.5}$).

The shrinkages measured after 28 days are presented in Figure 2 (b). It increased significantly with the GGBS concentration. However, adding MK to GGBS AAMs had a positive effect on shrinkage for both activation levels (15 or 25%). The shrinkage at 28 days was reduced from 2.4% ($A_{25}GGBS_{75}$) to 0.9%

(A₂₅MK_{62.5}GGBS_{12.5}) for high activation level and from 1.3% (A₁₅GGBS₈₅) to 0.5% (A₁₅MK_{72.5}GGBS_{12.5}) for low activation level. This positive result may be explained by the different setting times of MK and GGBS. Because of their highly porous structure, FCs are subject to high shrinkage [37]. Finding a binder with the lowest possible shrinkage is desirable to produce FC with good performance.

The compressive strengths measured after 28 days are presented in Figure 2 (c). Pure GGBS compressive strengths reached high values (83.7 and 110.5 MPa for A₂₅GGBS₇₅ and A₁₅GGBS₈₅, respectively). The highest compressive strength for the three AAMs that presented proper initial setting time was obtained with A₂₅MK_{62.5}GGBS_{12.5} (69.8 MPa at 28 days).

Acting on the proportions of MK and GGBS precursors enabled different AAMs properties to be obtained. However, as a minimum initial setting time was required, only 3 of the 14 mixes tested were suitable for AAM FC production. Among these three AAMs, A₂₅MK_{62.5}GGBS_{12.5} simultaneously presented the lowest shrinkage value (0.9% at 28 days) and the highest strength (69.8 MPa at 28 days). A₂₅MK_{62.5}GGBS_{12.5} was therefore chosen for AAM FC production.

4.2 AAM FC

The optimized mix (A₂₅MK_{62.5}GGBS_{12.5}) was used to produce AAM FC according to the experimental procedure presented in 3.4 (gas-foaming method). The use of a semi-rigid plastic sheet placed between the moulds and the samples resulted in a very good surface state of the FC lateral surface as presented in Figure 3 (a) (HP₁S_{0.008} samples, i.e. 1% of H₂O₂ and 0.008% of surfactant). However, some coalescence problems appeared in a few samples. When the fresh mineral suspension expanded due to the dioxygen released by the H₂O₂, bubbles could come into contact. Without surfactant, two bubbles could coalesce to form a single bubble. If surfactant was used, a membrane could appear between bubbles, preventing them from coalescing and thus stabilizing the FC until it set. If the surfactant content was too low, several membranes could break, leading to the creation of big bubbles that could escape from the fresh paste because of buoyancy force. However, coalescence does not always lead to collapse of the fresh porous structure if the bubbles remain small enough to stay trapped in the paste [38,39]. An example of FC (HP_{1.5}S_{0.001}) that suffered from excessive coalescence is presented in Figure 3 (b). When coalescence led to big bubbles rising to the surface, the amount of trapped air decreased and the fresh FC volume decreased, which explains the thin circular layer of AAMs observed. It indicates the maximum height reached by the FC before the fresh porous structure started to collapse. All FC produced with the lower surfactant content (0.001%) collapsed. Coalescence phenomena not only depended on surfactant content but also on H₂O₂ content. With the higher H₂O₂ content, the gas volume produced was

maximum and fresh FC stabilization required more surfactant as many bubbles came into contact. This explains why $HP_2S_{0.002}$ samples coalesced while samples with the same amount of surfactant but lower H_2O_2 content ($HP_1S_{0.002}$ and $HP_{1.5}S_{0.002}$) stayed stabilized until setting. It means that a minimum surfactant content is needed for each H_2O_2 content to prevent porous structure collapse.



Figure 3. (a) Samples after unmoulding ($HP_1S_{0.008}$); (b) $HP_{1.5}S_{0.001}$ samples with coalescence problems.

These collapsed FC were not characterized because they presented high densities for the amount of H_2O_2 employed and high conductivity. Moreover, producing FC with uncontrolled coalescence might be more difficult in an industrial process and lead to FCs with less controlled properties. Further discussion regarding these coalescence problems will be linked to the porous structure evaluation carried out in part 4.2.2.

4.2.1 Density

The unfoamed sample HP_0S_0 had an unmoulded density ρ_{um} of $1949 \pm 30 \text{ kg/m}^3$. After 7 days of drying, its dry density ρ_{dry} was $1673 \pm 26 \text{ kg/m}^3$, which corresponds to a mass loss of 14.4%. The AAM FC densities presented in Figure 4 (after unmoulding (a); after 7 days of drying (b)) show that low values were reached. After drying, all FC densities were between 250 and 500 kg/m^3 . Good reproducibility was achieved on densities (unmoulded and dry densities), as the coefficient of variation was always less than or equal to 3.1%. The mass loss of AAM FCs after 7 days of drying is presented in Table 5. It can be noted that all the samples lost $14.4 \pm 0.4\%$ of their initial mass. There was no influence of the H_2O_2 or surfactant content on mass loss. This may indicate that the interaction between H_2O_2 or surfactant and the MK-GGBS matrix microstructure was very limited as the mass loss was exactly the same.

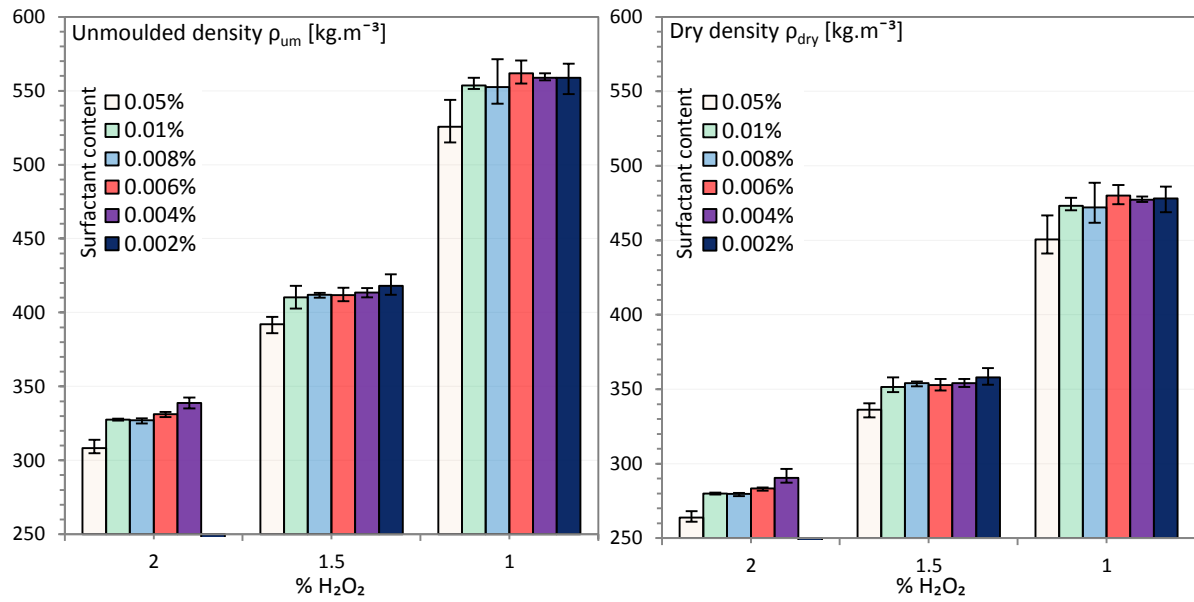


Figure 4. Effect of H₂O₂ and surfactant contents on the density of AAM FCs (a) after unmoulding and (b) after drying.

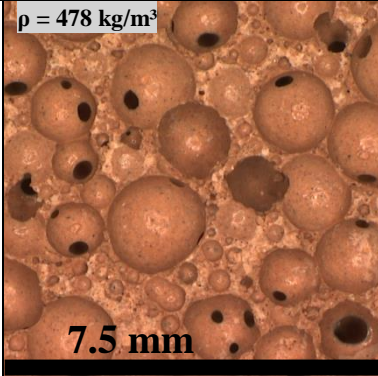
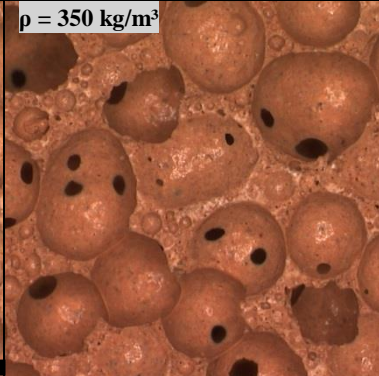
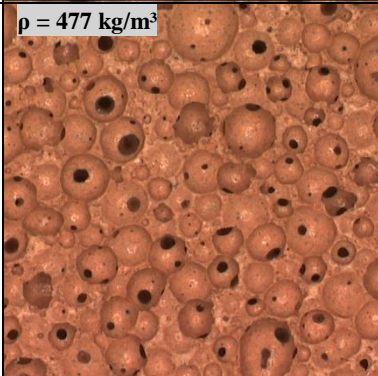
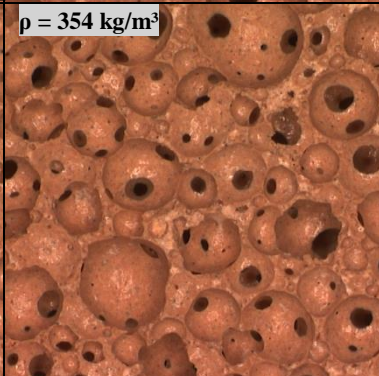
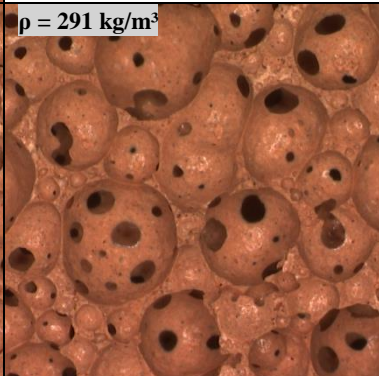
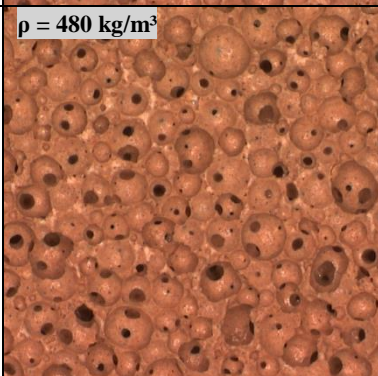
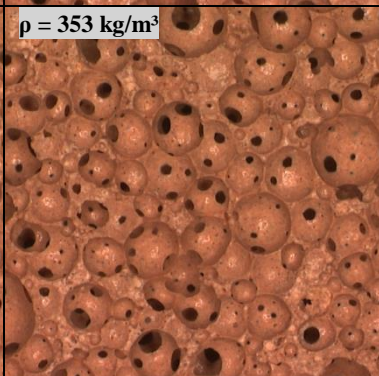
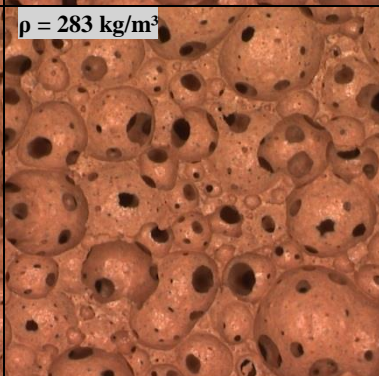
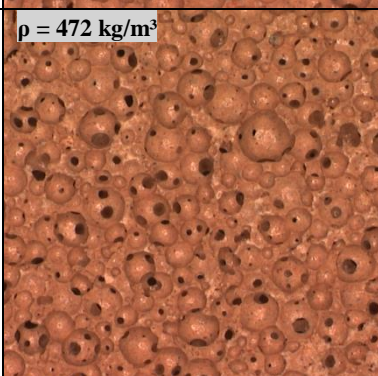
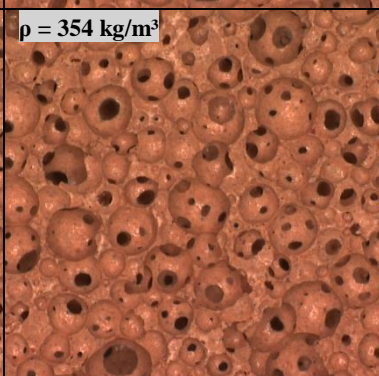
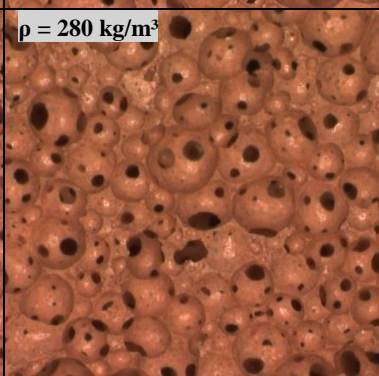
It can be noted in Figure 4 that the FC density mostly depended on the H₂O₂ content. However, surfactant content also impacted FC density. Adding surfactant tended to decrease the FC density, meaning that some air was already entrained and stabilized through the paste during mixing. Some FC were produced by quick mixing [12,40] of a paste that contained a high amount of surfactant (mix-foaming method). However, the pre-foaming method is usually preferred to the mix-foaming method because it requires less surfactant and is easier to set up on a construction site [41]. Here, surfactant content remained small, explaining why density variation remained small. Adding more surfactant could theoretically enable a lower density to be reached. However, as part 4.2.4 will show, high surfactant content was detrimental to the FC mechanical properties.

4.2.2 Porous structure

The significant influence of H₂O₂ and surfactant contents on porous structure is presented in Figure 5. Each picture corresponds to a FC surface of 7.5² mm². The FC samples produced with the lower surfactant content (0.001%) suffered from coalescence that led to fresh porous structure collapse and thus did not satisfy the requirements for good FC production. This is why their porous structures are not presented in Figure 5. With fixed surfactant content, a change of H₂O₂ content had a strong influence on FC density (Figure 4) and the porous structure was also modified. The initial amount of entrained air was assumed to be the same, as the surfactant content was the same. Increasing H₂O₂ content led to a less stable FC due to the large amount of gas produced. More bubble membranes were created, leading to an interconnected porous structure.

At low surfactant content ($HP_1S_{0.002}$ and $HP_{1.5}S_{0.002}$) some bubbles were quite big (diameter > 1.8 mm, deduced from the size of the pictures - 7.5 mm). The porous structure observed for these compositions was the equilibrium state achieved when the paste set. When the gas-off started, only a few small bubbles (entrained air) were trapped through the paste. At the beginning of the gas-off, numerous tiny bubbles appeared in the paste and started to grow. After a moment (depending on the H_2O_2 content), these small bubbles came in contact and membranes appeared between them because of the surfactant action. However, with low surfactant content, membranes could be broken, which tended to reduce the number of bubbles and increase their average diameter. A new equilibrium state was achieved and was maintained until the next coalescence. The number of coalescence occurrences decreased with increasing surfactant content. Thus, for a given H_2O_2 content, the higher surfactant content was associated with a thinner and more homogenous porous structure.

Thus, controlling both H_2O_2 and surfactant contents allows FC with controlled density and porous structure to be produced. Porous structure modification might have an impact on the thermomechanical properties and will be discussed later. Controlling the porous structure may also be very interesting for other applications such as filtration [42] or energy storage systems [43,44]. This is a new result because FCs presented in the literature were produced with constant surfactant content, their porous structure usually being controlled by H_2O_2 content or paste rheology.

| | | H ₂ O ₂ content | | |
|--------------------|---------|---|--|---|
| | | 1 % | 1,5 % | 2 % |
| Surfactant content | |  <p>$\rho = 478 \text{ kg/m}^3$</p> <p>7.5 mm</p> |  <p>$\rho = 350 \text{ kg/m}^3$</p> | Coalescence |
| | 0.004 % |  <p>$\rho = 477 \text{ kg/m}^3$</p> |  <p>$\rho = 354 \text{ kg/m}^3$</p> |  <p>$\rho = 291 \text{ kg/m}^3$</p> |
| | 0.006% |  <p>$\rho = 480 \text{ kg/m}^3$</p> |  <p>$\rho = 353 \text{ kg/m}^3$</p> |  <p>$\rho = 283 \text{ kg/m}^3$</p> |
| | 0.008% |  <p>$\rho = 472 \text{ kg/m}^3$</p> |  <p>$\rho = 354 \text{ kg/m}^3$</p> |  <p>$\rho = 280 \text{ kg/m}^3$</p> |

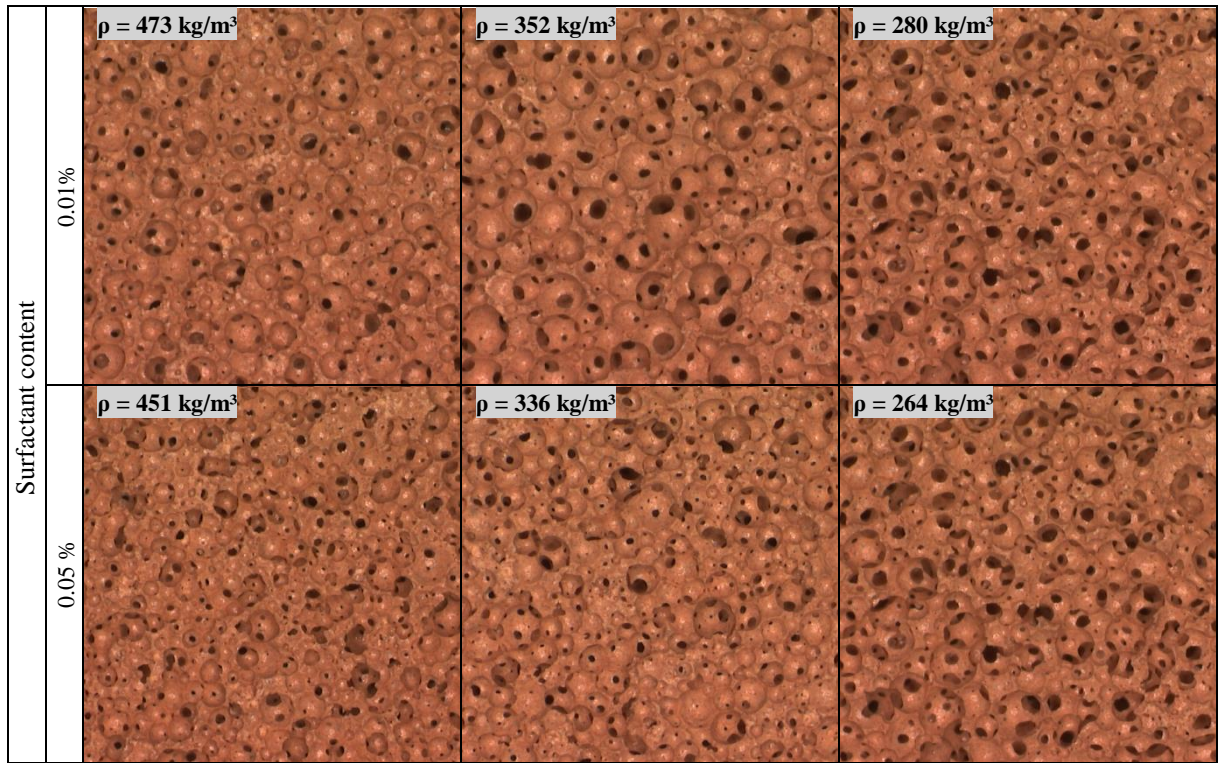


Figure 5. Porous structure evolution depending on H_2O_2 and surfactant contents. Each picture corresponds to $7.5 \times 7.5 \text{ mm}^2$.

4.2.3 Thermal conductivity

The FC thermal conductivity results are presented in Figure 6. All thermal conductivities were below 0.14 W/(m.K). Excellent reproducibility was found, as the thermal conductivity coefficient of variation was always lower than or equal to 2.6% (Table 5). Thermal conductivity values decreased with decreasing density, and the density varied with the H₂O₂ addition. At constant H₂O₂ content, the density was nearly stable. Thermal conductivity decreased a little with surfactant content increase (Figure 4 (b)). This may, for example, explain why the thermal conductivity value of HP_{1.5}S_{0.05} ($\rho = 336 \text{ kg/m}^3$; $\lambda = 0.099 \text{ W/(m.K)}$) was lower than the thermal conductivity of HP_{1.5}S_{0.002} ($\rho = 358 \text{ kg/m}^3$; $\lambda = 0.113 \text{ W/(m.K)}$). However, at a given H₂O₂ content, thermal conductivity varied more (14.1%) than density did (6.5%) when the surfactant content moved from its lowest value to its highest (0.002 to 0.05%). This difference can only be explained by the strong modification of the porous structure presented in Figure 5. Thermal conductivity characterizes the ability of a material to transfer heat energy. The FCs produced were composed of an AAM matrix (HP₀S₀, $\rho = 1950 \text{ kg/m}^3$; $\lambda = 1.12 \text{ W/(m.K)}$ - Table 4) and air, with low thermal conductivity ($\rho = 1.2 \text{ kg/m}^3$; $\lambda = 0.025 \text{ W/(m.K)}$ at 20°C)). The matrix/air thermal conductivity ratio was around 45, which means that almost all the heat would be transferred through the solid matrix, which had the higher thermal conductivity. Because of the small size of the pores, natural convection can be neglected [45]. Increasing surfactant content, at fixed H₂O₂ content, promoted a thin porous structure. The tortuosity of such FC will be higher than the tortuosity of an FC produced with lower surfactant content. Pore tortuosity can be defined as the ratio of the effective path length to the sample length [46]. Heat transfer will be slowed by high tortuosity (high surfactant content). Thus, using high surfactant content seems to be appropriate to produce FC with good thermal insulation ability.

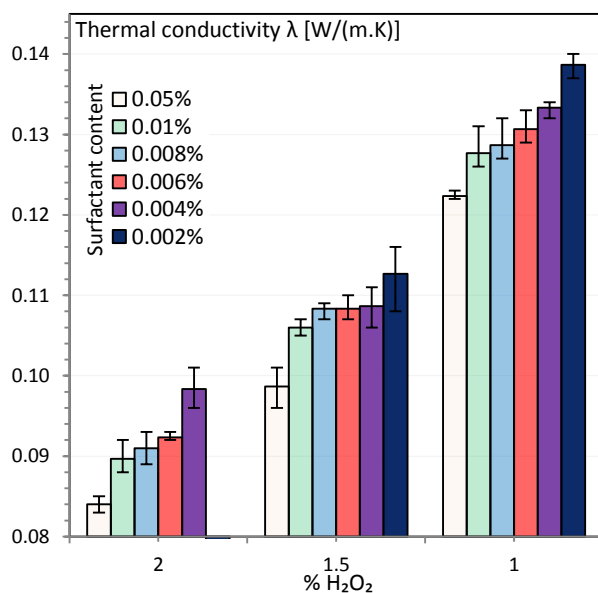


Figure 6. Effect of H₂O₂ and surfactant contents on AAM FCs thermal conductivity.

In a recent paper, Samson et al. [40] presented the thermomechanical performance of classic lightweight concrete (lightweight aggregate concrete and FC). Classic FC was FC produced with binder that was not alkali-activated (cement, gypsum, etc.). The thermomechanical properties of classic FC are presented in Figure 7. For the sake of clarity, all the data concerning classic FC have the same symbol (small grey squares) in Figure 7. Different markers are used for AAM FCs (information concerning these FCs is presented in Table 5). As can be seen in Figure 7, regardless of the binder used, thermal conductivity is highly correlated to density. The AAM FCs produced (filled red squares) presented low thermal conductivity in agreement with the low densities reached.

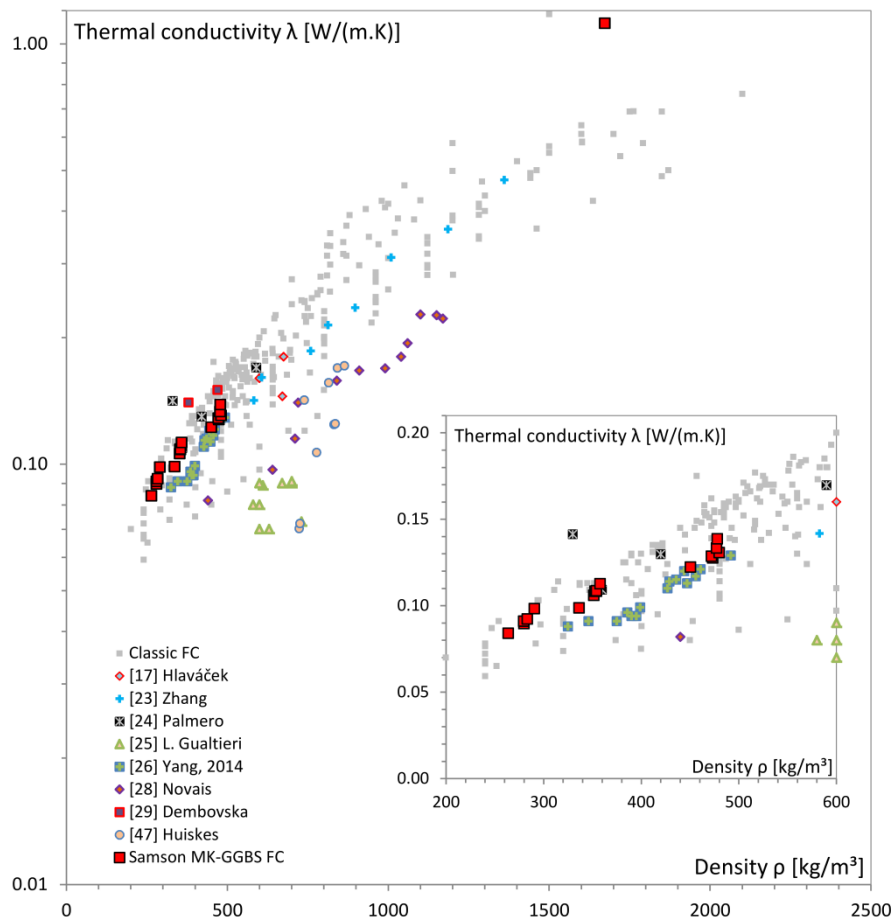


Figure 7. Comparison of the thermal conductivity values obtained in the literature [17,23–26,28,29,40,47] and in this study.

4.2.4 Compressive strength

The compressive strength results are presented in Figure 8. Most samples reached interesting compressive strengths. The highest was achieved by $HP_1S_{0.004}$ ($f_c = 3.34$ MPa; $\rho = 477$ kg/m³). Compressive strength mostly depends on density; the FC produced with 2% of H₂O₂ had the lowest densities. However, for a given H₂O₂ content, compressive strength was sensitive to surfactant content. A maximum compressive strength was obtained with 0.004% of surfactant, for different H₂O₂ contents (1, 1.5 and 2%). This dosage can be considered to be the optimized surfactant content. For example, with 2% of H₂O₂, the highest compressive strength was obtained by $HP_2S_{0.004}$ ($\rho = 477$ kg/m³; $f_c = 3.34$ MPa), while adding ($HP_2S_{0.006}$; $\rho = 480$ kg/m³; $f_c = 3.05$ MPa) or decreasing ($HP_2S_{0.002}$; $\rho = 478$ kg/m³; $f_c = 3.05$ MPa) the surfactant content led to lower compressive strength. Simply by changing surfactant content, the compressive strength was increased by around 10%, at a constant FC density. With high surfactant content FC ($HP_2S_{0.05}$; $\rho = 451$ kg/m³; $f_c = 2.24$ MPa), the density decreased by 5% and the compressive strength decreased by 33% with respect to the value obtained with the optimized surfactant content. As described in part 4.2.2, the porous structure evolved significantly with surfactant content. The porous structure of $HP_2S_{0.002}$ comprised several big bubbles that could act as local defects and cause premature failure of the FC (Figure 5). Doubling the surfactant content ($HP_2S_{0.004}$) strongly reduced the average radius of bubbles, giving a more homogeneous porous structure that presented higher compressive strength. Adding more surfactant reduced the average bubble radius further. Bubbles were more numerous, more connected and separated by thinner matrix walls. The load-bearing ability was decreased. This revealed that the optimized surfactant content of FC should be carefully determined to obtain FC with high compressive strength. Adding a lot of surfactant prevented coalescence problems but the porous structure was not optimized for bearing ability. For the optimized surfactant content, some coalescence occurred, leading to a homogeneous porous structure with medium diameter bubbles separated by wide matrix walls. The coalescence was controlled and optimized. It is possible that excessive surfactant content could also hinder alkali-activation of precursors.

The optimized dosage found was the same for the three H₂O₂ contents. However, it can be guessed that there is a single optimal surfactant content for each density (each H₂O₂ content) [48]. The single optimal surfactant content should decrease with increasing H₂O₂ content. Further investigations with several surfactant contents around the optimized value could help to check if this hypothesis is correct.

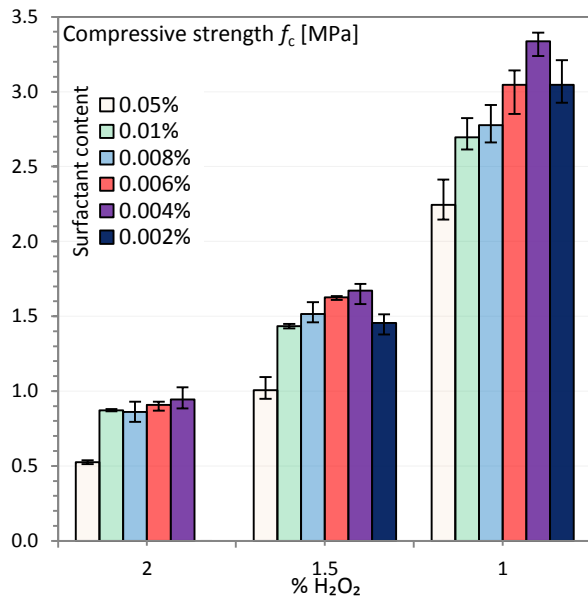


Figure 8. Effect of H_2O_2 and surfactant contents on AAM FCs compressive strength.

The compressive strength values obtained are compared to those for classic FC and AAM FCs in Figure 9. The FCs produced (filled red squares) exhibit good compressive strength considering their low densities. The FCs produced here present competitive results relative to both classic FC and AAM FCs.

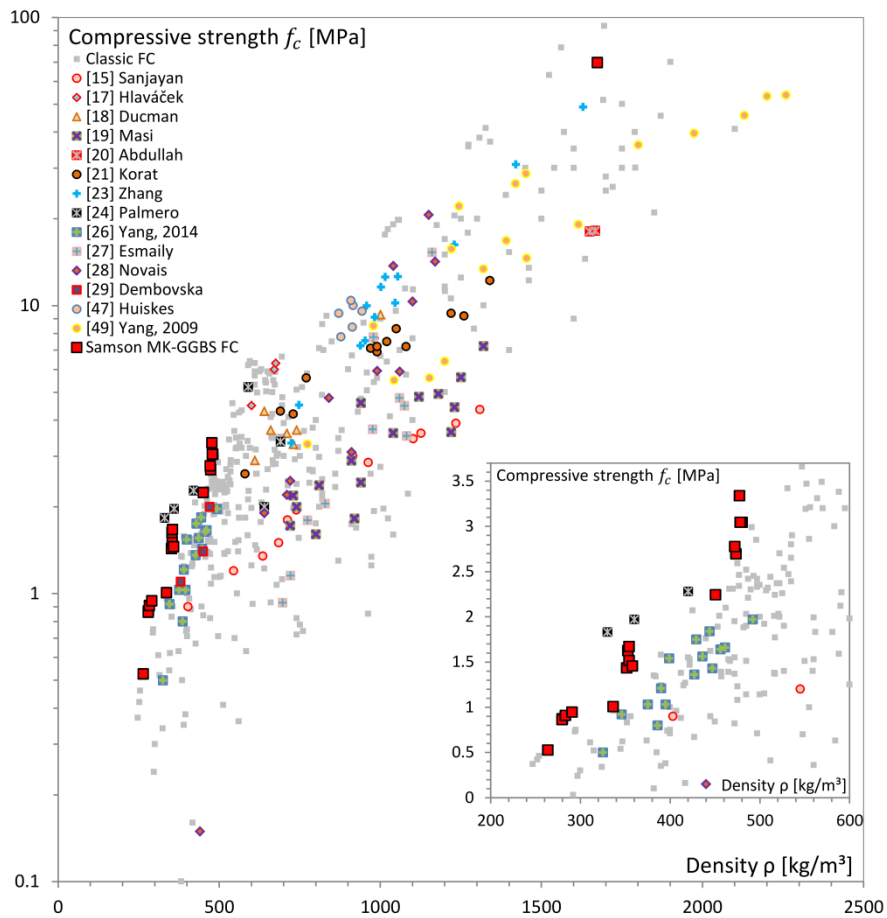


Figure 9. Comparison of the compressive strength values obtained in the literature [15,17–21,23,24,26–29,40,47,49] and in this study.

5 Conclusion

This study starts with the identification of optimized proportions between MK, GGBS and activator. The produced AAM matrix must present interesting mechanical capacity and moderate shrinkage. Moreover, AAM matrix should start to set after the end of H₂O₂ gas-off (180 minutes) which is used to create AAM FC porosity. The retained matrix composition (A₂₅MK_{62.5}GGBS_{12.5}) is then employed for AAM FC production. The influence of two main parameters (H₂O₂ and surfactant contents) on AAM properties (density, porous structure, thermal conductivity and compressive strength) were investigated. Lightweight AAMs were obtained with density from 264 to 480 kg/m³. The following findings were made:

- FC density mostly depends on H₂O₂ content. However, surfactant content also influences FC density because adding more surfactant results in more air being entrained during paste production, before H₂O₂ insertion. However, this influence was much weaker than that of H₂O₂.
- The FC porous structure depends greatly on both H₂O₂ and surfactant contents. High surfactant content FCs have a thin homogenous porous structure. Stable surfactant membranes were created between bubbles, which stabilized the porous structure. Reducing surfactant content led to FCs with larger bubbles, meaning that some coalescence occurred. Below a certain surfactant level, the fresh porous structure was not stabilized until the AAM matrix set and so the FC collapsed.
- FC thermal conductivity ranges between 0.084 and 0.139 W/(m.K). FC thermal conductivity mostly depends on FC density and surfactant content in a lesser extent. At constant density, thermal conductivity was decreased by high tortuosity (high surfactant content).
- FC compressive strength ranges between 0.53 and 3.34 MPa. It mainly depends on H₂O₂ content. At constant density, FC compressive strength depends on surfactant content. An optimized surfactant content (0.004%) maximizing FC compressive strength at constant density was found.
- The FC produced exhibited competitive compressive strength in comparison with the FC found in the literature.

6 References

- [1] P. Duxson, A. Fernández-Jiménez, J.L. Provis, G.C. Lukey, A. Palomo, J.S.J. van Deventer, Geopolymer technology: the current state of the art, *J. Mater. Sci.* 42 (2006) 2917–2933. doi:10.1007/s10853-006-0637-z.
- [2] J. L. Provis, J.S.J. Van Deventer, Alkali Activated Materials - State-of-the-Art Report, RILEM TC | John Provis | Springer, Springer, n.d. <http://www.springer.com/us/book/9789400776715> (accessed May 5, 2017).
- [3] J.L. Provis, A. Palomo, C. Shi, Advances in understanding alkali-activated materials, *Cem. Concr. Res.* 78, Part A (2015) 110–125. doi:10.1016/j.cemconres.2015.04.013.
- [4] F. Pacheco-Torgal, Z. Abdollahnejad, A.F. Camões, M. Jamshidi, Y. Ding, Durability of alkali-activated binders: A clear advantage over Portland cement or an unproven issue?, *Constr. Build. Mater.* 30 (2012) 400–405. doi:10.1016/j.conbuildmat.2011.12.017.
- [5] S.A. Bernal, E.D. Rodríguez, R.M. de Gutiérrez, M. Gordillo, J.L. Provis, Mechanical and thermal characterisation of geopolymers based on silicate-activated metakaolin/slag blends, *J. Mater. Sci.* 46 (2011) 5477–5486. doi:10.1007/s10853-011-5490-z.
- [6] M.C. Bignozzi, S. Manzi, I. Lancellotti, E. Kamseu, L. Barbieri, C. Leonelli, Mix-design and characterization of alkali activated materials based on metakaolin and ladle slag, *Appl. Clay Sci.* 73 (2013) 78–85. doi:10.1016/j.clay.2012.09.015.
- [7] A. Buchwald, H. Hilbig, C. Kaps, Alkali-activated metakaolin-slag blends—performance and structure in dependence of their composition, *J. Mater. Sci.* 42 (2007) 3024–3032. doi:10.1007/s10853-006-0525-6.
- [8] S.A. Bernal, E.D. Rodríguez, R.M. de Gutiérrez, J.L. Provis, S. Delvasto, Activation of Metakaolin/Slag Blends Using Alkaline Solutions Based on Chemically Modified Silica Fume and Rice Husk Ash, *Waste Biomass Valorization.* 3 (2011) 99–108. doi:10.1007/s12649-011-9093-3.
- [9] G. Samson, M. Cyr, X.X. Gao, Formulation and characterization of blended alkali-activated materials based on flash-calcined metakaolin, fly ash and GGBS, *Constr. Build. Mater.* 144 (2017) 50–64. doi:10.1016/j.conbuildmat.2017.03.160.
- [10] P.H.R. Borges, N. Banthia, H.A. Alcamand, W.L. Vasconcelos, E.H.M. Nunes, Performance of blended metakaolin/blastfurnace slag alkali-activated mortars, *Cem. Concr. Compos.* 71 (2016) 42–52. doi:10.1016/j.cemconcomp.2016.04.008.
- [11] J. Jiang, Z. Lu, Y. Niu, J. Li, Y. Zhang, Study on the preparation and properties of high-porosity foamed concretes based on ordinary Portland cement, *Mater. Des.* 92 (2016) 949–959. doi:10.1016/j.matdes.2015.12.068.
- [12] K. Ramamurthy, E.K. Kunhanandan Nambiar, G. Indu Siva Ranjani, A classification of studies on properties of foam concrete, *Cem. Concr. Compos.* 31 (2009) 388–396. doi:10.1016/j.cemconcomp.2009.04.006.
- [13] F.K. Akthar, J.R.G. Evans, High porosity (> 90%) cementitious foams, *Cem. Concr. Res.* 40 (2010) 352–358. doi:10.1016/j.cemconres.2009.10.012.
- [14] J. Feng, R. Zhang, L. Gong, Y. Li, W. Cao, X. Cheng, Development of porous fly ash-based geopolymer with low thermal conductivity, *Mater. Des.* 1980-2015. 65 (2015) 529–533. doi:10.1016/j.matdes.2014.09.024.
- [15] J.G. Sanjayan, A. Nazari, L. Chen, G.H. Nguyen, Physical and mechanical properties of lightweight aerated geopolymer, *Constr. Build. Mater.* 79 (2015) 236–244. doi:10.1016/j.conbuildmat.2015.01.043.
- [16] E. Kamseu, Z.N.M. NGouloure, B.N. Ali, S. Zekeng, U.C. Melo, S. Rossignol, C. Leonelli, Cumulative pore volume, pore size distribution and phases percolation in porous inorganic polymer composites: Relation microstructure and effective thermal conductivity, *Energy Build.* 88 (2015) 45–56. doi:10.1016/j.enbuild.2014.11.066.
- [17] P. Hlaváček, V. Šmilauer, F. Škvára, L. Kopecký, R. Šulc, Inorganic foams made from alkali-activated fly ash: Mechanical, chemical and physical properties, *J. Eur. Ceram. Soc.* 35 (2015) 703–709. doi:10.1016/j.jeurceramsoc.2014.08.024.

- [18] V. Ducman, L. Korat, Characterization of geopolymer fly-ash based foams obtained with the addition of Al powder or H₂O₂ as foaming agents, *Mater. Charact.* 113 (2016) 207–213. doi:10.1016/j.matchar.2016.01.019.
- [19] G. Masi, W.D.A. Rickard, L. Vickers, M.C. Bignozzi, A. van Riessen, A comparison between different foaming methods for the synthesis of light weight geopolymers, *Ceram. Int.* 40 (2014) 13891–13902. doi:10.1016/j.ceramint.2014.05.108.
- [20] M.M. Al Bakri Abdullah, K. Hussin, M. Bnhussain, K.N. Ismail, Z. Yahya, R.A. Razak, Fly Ash-based Geopolymer Lightweight Concrete Using Foaming Agent, *Int. J. Mol. Sci.* 13 (2012) 7186–7198. doi:10.3390/ijms13067186.
- [21] L. Korat, V. Ducman, The influence of the stabilizing agent SDS on porosity development in alkali-activated fly-ash based foams, *Cem. Concr. Compos.* 80 (2017) 168–174. doi:10.1016/j.cemconcomp.2017.03.010.
- [22] Z. Zhang, H. Wang, The Pore Characteristics of Geopolymer Foam Concrete and Their Impact on the Compressive Strength and Modulus, *Struct. Mater.* (2016) 38. doi:10.3389/fmats.2016.00038.
- [23] Z. Zhang, J.L. Provis, A. Reid, H. Wang, Mechanical, thermal insulation, thermal resistance and acoustic absorption properties of geopolymer foam concrete, *Cem. Concr. Compos.* 62 (2015) 97–105. doi:10.1016/j.cemconcomp.2015.03.013.
- [24] P. Palmero, A. Formia, P. Antonaci, S. Brini, J.-M. Tulliani, Geopolymer technology for application-oriented dense and lightened materials. Elaboration and characterization, *Ceram. Int.* 41 (2015) 12967–12979. doi:10.1016/j.ceramint.2015.06.140.
- [25] M. Lassinantti Gualtieri, M. Romagnoli, A.F. Gualtieri, Preparation of phosphoric acid-based geopolymer foams using limestone as pore forming agent – Thermal properties by in situ XRPD and Rietveld refinements, *J. Eur. Ceram. Soc.* 35 (2015) 3167–3178. doi:10.1016/j.jeurceramsoc.2015.04.030.
- [26] K.-H. Yang, K.-H. Lee, J.-K. Song, M.-H. Gong, Properties and sustainability of alkali-activated slag foamed concrete, *J. Clean. Prod.* 68 (2014) 226–233. doi:10.1016/j.jclepro.2013.12.068.
- [27] H. Esmaily, H. Nuranian, Non-autoclaved high strength cellular concrete from alkali activated slag, *Constr. Build. Mater.* 26 (2012) 200–206. doi:10.1016/j.conbuildmat.2011.06.010.
- [28] R.M. Novais, G. Ascensão, L.H. Buruberri, L. Senff, J.A. Labrincha, Influence of blowing agent on the fresh- and hardened-state properties of lightweight geopolymers, *Mater. Des.* 108 (2016) 551–559. doi:10.1016/j.matdes.2016.07.039.
- [29] L. Dembovska, D. Bajare, V. Ducman, L. Korat, G. Bumanis, The use of different by-products in the production of lightweight alkali activated building materials, *Constr. Build. Mater.* 135 (2017) 315–322. doi:10.1016/j.conbuildmat.2017.01.005.
- [30] R. Pouhet, Formulation and durability of metakaolin-based geopolymers, PhD Thesis, LMDC Toulouse, France, 2015.
- [31] N.K. Lee, J.G. Jang, H.K. Lee, Shrinkage characteristics of alkali-activated fly ash/slag paste and mortar at early ages, *Cem. Concr. Compos.* 53 (2014) 239–248. doi:10.1016/j.cemconcomp.2014.07.007.
- [32] Z. Zuhua, Y. Xiao, Z. Huajun, C. Yue, Role of water in the synthesis of calcined kaolin-based geopolymer, *Appl. Clay Sci.* 43 (2009) 218–223. doi:10.1016/j.clay.2008.09.003.
- [33] ASTM C191 - 01, ASTM C191 - 01 - Standard Test Method for Time of Setting of Hydraulic Cement by Vicat Needle, (2006).
- [34] ASTM C596 - 09e1, ASTM C596 - 09e1 - Standard Test Method for Drying Shrinkage of Mortar Containing Hydraulic Cement, (2001).
- [35] K. Gao, K.-L. Lin, D. Wang, C.-L. Hwang, H.-S. Shiu, Y.-M. Chang, T.-W. Cheng, Effects SiO₂/Na₂O molar ratio on mechanical properties and the microstructure of nano-SiO₂ metakaolin-based geopolymers, *Constr. Build. Mater.* 53 (2014) 503–510. doi:10.1016/j.conbuildmat.2013.12.003.
- [36] C. Li, H. Sun, L. Li, A review: The comparison between alkali-activated slag (Si + Ca) and metakaolin (Si+Al) cements, *Cem. Concr. Res.* 40 (2010) 1341–1349.
- [37] P. Chindaprasirt, U. Rattanasak, Shrinkage behavior of structural foam lightweight concrete containing glycol compounds and fly ash, *Mater. Des.* 32 (2011) 723–727. doi:10.1016/j.matdes.2010.07.036.

- [38] N. Dubash, I. Frigaard, Conditions for static bubbles in viscoplastic fluids, *Phys. Fluids*. 16 (2004) 4319–4330. doi:10.1063/1.1803391.
- [39] G. Samson, Phelipot-Mardelé, C. Lanos, Static bubble behavior in a yield stress fluid, in: 5th Int. Conf. Biofoams, Sorrento, Italy, 2015.
- [40] G. Samson, A. Phelipot-Mardelé, C. Lanos, A review of thermomechanical properties of lightweight concrete, *Mag. Concr. Res.* (2016).
- [41] K. Buyn, H. Song, S. Sark, Development of structural lightweight foamed concrete using polymer foam agent, (2016) 9.
- [42] M. Strozi Cilla, P. Colombo, M. Raymundo Morelli, Geopolymer foams by gelcasting, *Ceram. Int.* 40 (2014) 5723–5730. doi:10.1016/j.ceramint.2013.11.011.
- [43] K. Ndiaye, S. Ginestet, M. Cyr, Modelling and experimental study of low temperature energy storage reactor using cementitious material, *Appl. Therm. Eng.* 110 (2017) 601–615. doi:10.1016/j.applthermaleng.2016.08.157.
- [44] K. Ndiaye, M. Cyr, S. Ginestet, Durability and stability of an ettringite-based material for thermal energy storage at low temperature, *Cem. Concr. Res.* 99 (2017) 106–115. doi:10.1016/j.cemconres.2017.05.001.
- [45] T.W. Clyne, I.O. Golosnoy, J.C. Tan, A.E. Markaki, Porous materials for thermal management under extreme conditions, *Philos. Transact. A Math. Phys. Eng. Sci.* 364 (2006) 125–146. doi:10.1098/rsta.2005.1682.
- [46] R. Zhong, M. Xu, R. Vieira Netto, K. Wille, Influence of pore tortuosity on hydraulic conductivity of pervious concrete: Characterization and modeling, *Constr. Build. Mater.* 125 (2016) 1158–1168. doi:10.1016/j.conbuildmat.2016.08.060.
- [47] D.M.A. Huiskes, A. Keulen, Q.L. Yu, H.J.H. Brouwers, Design and performance evaluation of ultra-lightweight geopolymer concrete, *Mater. Des.* 89 (2016) 516–526. doi:10.1016/j.matdes.2015.09.167.
- [48] G. Samson, Synthèse et propriétés de mousses minérales, PhD Thesis, INSA Rennes, 2015.
- [49] K.-H. Yang, J.-K. Song, J.-S. Lee, Properties of alkali-activated mortar and concrete using lightweight aggregates, *Mater. Struct.* 43 (2009) 403–416. doi:10.1617/s11527-009-9499-6.